Proceedings of FUELCELL2006
The 4th International Conference on FUEL CELL SCIENCE, ENGINEERING and TECHNOLOGY
June 19-21, 2006, Irvine, CA

FUELCELL2006-97177

PARAMETERIZATION OF FUEL CELL STACK VOLTAGE: ISSUES ON SENSITIVITY, CELL-TO-CELL VARIATION, AND TRANSIENT RESPONSE

Arlette L. Schilter
Measurement and Control Laboratory
Swiss Federal Institute of Technology Zurich (ETH)
Zurich, Switzerland
Email: aschilter@alumni.ethz.ch

Denise A. McKay, Anna G. Stefanopoulou
Fuel Cell Control Systems Laboratory
The University of Michigan
Ann Arbor, Michigan, 48109
Email: dmckay@umich.edu, annastef@umich.edu

ABSTRACT

We present here a calibrated and experimentally validated lumped parameter model of fuel cell polarization for a hydrogen fed multi-cell, low-pressure, proton exchange membrane (PEM) fuel cell stack. The experimental methodology devised for calibrating the model was completed on a 24 cell, 300 cm^2 stack with GORE^{TM} PRIMERA® Series 5620 membranes. The predicted cell voltage is a static function of current density, stack temperature, reactant partial pressures, and membrane water content. The maximum prediction error associated with the sensor resolutions used for the calibration is determined along with a discussion of the model sensitivity to physical variables. The expected standard deviation due to the cell-to-cell voltage variation is also modelled.

In contrast to other voltage models that match the observed dynamic voltage behavior by adding unreasonably large double layer capacitor effects or by artificially adding dynamics to the voltage equation, we show that a static model can be used when combined with dynamically resolved variables. The developed static voltage model is then connected with a dynamic fuel cell system model that includes gas filling dynamics, diffusion and water dynamics and we demonstrate the ability of the static voltage equation to predict important transients such as reactant depletion and electrode flooding. It is shown that the model can qualitatively predict the observed stack voltage under various operating conditions including step changes in current, temperature variations, and anode purging.

INTRODUCTION

The operating voltage of a fuel cell stack determines the stack efficiency. Moreover, the stack voltage can provide indirect information about many important fuel cell variables. As increased attention is applied in understanding the reactant and water dynamics in proton exchange membrane (PEM) fuel cells, the impact of transients such as reactant depletion or electrode flooding on the cell efficiency can be examined by observing the cell voltage. For this reason, an accurate model of cell average voltage and the expected cell-to-cell variations are very important for control and diagnostic purposes. Additionally, an accurate model of cell voltage provides a means for model calibration [11, 13, 14].

Numerous low order, physics based models have been developed to predict the cell operating voltage. Springer [16] published an isothermal, one-dimensional, steady-state model for a single cell, demonstrating the influence of membrane water content on polarization. Amphlett et al. [1] determined tunable parameters for the polarization and validated the model with a 35-cell stack. Mann and Amphlett [9] then developed a generic steady-state empirical model for the cell polarization with active area and membrane thickness as inputs in the ohmic overvoltage, and validated it with data for different fuel cell systems. Our work is similar to [14] where the averaged cell voltage of 0.6 kW fuel cell stack was parameterized and a standard deviation based on the observed cell-to-cell variations was derived.

Two and three dimensional models have been used to quantify the steady state polarization. These high order models often calculate along the channel temperature and reactant concen-

trations but ultimately use spatially averaged inputs to a voltage model that calculates an averaged cell voltage [5, 17, 2]. These low and high order models all use static equations for the cell voltage as a function of physical measurements. When the inputs to the model are dynamic, the predicted voltage response is then dynamic. Our work is similar to [14,15] where the averaged cell voltage of a 6 kW PEMFC stack was parameterized under standard conditions based on the observed cell-to-cell variations.

Rather than generate a detailed physics based model to describe the fuel cell system dynamics, work has been completed to account for dynamics directly in the voltage model. Correa [4] uses a charge double layer to add dynamics to activation and concentration losses. Other work [12, 7] add a first order derivative to the polarization similar to [4]. These additional dynamics can then account for the transient voltage response during step changes in current. In [6] the impact of reactant stoichiometry on cell voltage following step changes in current was examined. First order dynamics are then used to describe the transfer function from voltage to current, with current as a state variable. In [3] the constants of the electrical components of an equivalent circuit are estimated using electrochemical impedance studies to describe the voltage dynamics.

Pukrushpan [13] parameterizes a low order, control-oriented fuel cell system model that captures reactant dynamics during load transients based on a generalized steady-state electrochemical model produced by Mann [9]. This paper modifies and reparameterizes the voltage model in [13] for a low pressure, 24 cell, 300 cm^2 PEM fuel cell stack with Gore^{TM} PRIMERA® Series 5620 membranes. The predicted cell voltage is a function of current density, stack temperature, reactant partial pressure, and membrane water content. The parameters of this nonlinear function have been identified based on measurements taken at the fuel cell lab at University of Michigan. We then demonstrate the ability of this static voltage equation to capture the voltage degradation during reactant depletion and electrode flooding by coupling the static voltage equation with the dynamic fuel cell model developed in [11] which includes the diffusion dynamics of oxygen, hydrogen, and vapor in the liquid saturated GDL.

NOMENCLATURE

A_{fc} Fuel cell active area, [m^2]
E Reversible cell voltage, [V]
F Faraday constant, 96485 C/mol
ΔG^0 Standard Gibbs free energy, -237000 J/mol
I Current, [A]
i Current density, [mA/cm^2], [A/m^2]
M_{mol} Molar mass, g/mol
n_c Number of cells in the stack, [-]
p_{H_2} Hydrogen partial pressure, [Pa]
p_{O_2} Oxygen partial pressure, [Pa]
p_{sat} Saturation pressure, [Pa]
p^0 Standard pressure, 1 atm, 101325 Pa
R Universal gas constant, 8.314510 J/mol·K
ΔS^0 Standard entropy, -44.43 J/mol·K
T Temperature, [K]
T^0 Standard temperature, 25°C, 298.15 K
U Voltage, also operational voltage, [V]
W Mass flow, [kg/s]
y_{O_2} Oxygen mole fraction in dry air, [-]
Δ Change, [-]
λ Air excess ratio, [-]
λ_m Membrane water content, [-]
ϕ Humidity, [-]

Subscripts:

an Anode
act Activation loss
ave Average
ca Cathode
cell Cell property
conc Concentration loss
in Inlet
out Outlet
ohmic Ohmic loss
st Stack
v Vapor

1 MODELLING CELL VOLTAGE

The physically motivated basis function for the parameter identification of the polarization was taken from [13] and is reproduced here for clarity. The operational cell voltage, U, is a combination of the open circuit voltage, E, the activation loss, U_{act}, the ohmic loss, U_{ohmic}, and the concentration loss, U_{conc} shown by:

$$U = E - U_{act} - U_{ohmic} - U_{conc} \tag{1}$$

The open circuit voltage, E, is derived from electrochemical theory, and described by:

$$E = \frac{-\Delta G^0}{2F} + \frac{\Delta S^0}{2F}(T_{st} - T^0) + \frac{R \cdot T_{st}}{2F} ln\left(\frac{p_{H_2} \cdot p_{O_2}^{0.5}}{(p^0)^{1.5}}\right) \tag{2}$$

$$= 1.23 - 2.30 \cdot 10^{-4} \cdot (T_{st} - 298.15) + 4.3 \cdot 10^{-5} \cdot T_{st} \cdot ln\left(\frac{p_{H_2} \cdot p_{O_2}^{0.5}}{(101325)^{1.5}}\right). \tag{3}$$

Where ΔG^0 is the Gibb's free energy, ΔS^0 the standard entropy, F the Faraday constant, R the universal gas constant, T_{st} the stack temperature, p_{H_2} the hydrogen partial pressure, p_{O_2} the oxygen partial pressure, and p^0 and T^0 standard conditions.

The polarization curve is often plotted as a function of current density, *i*. This eases the comparison between fuel cells with different active areas. When the catalyst layers are free form liquid water accumulations, current density can be calculated with:

$$i = \frac{I}{A_{fc}} \tag{4}$$

where I is the total current produced by the electrons from the reaction, and A_{fc} the active fuel cell area of the membrane.

Overvoltage, losses, or irreversibilities, arise from reaction kinetics (in the activation region at low current density) and membrane resistance (in the ohmic ohmic region at moderate current density). In regions with high current density the concentration loss decreases the cell voltage rapidly. This loss appears due to transport limitations in the channels. No experiments were collected in this current range.

The activation energy determines the reaction rate. When current is demanded, additional energy is needed to accelerate the chemical reaction, causing a rapid voltage drop called activation loss. Tafel discovered a logarithmic relationship between the voltage drop and the current for the activation. McDougall showed that one of Tafel's parameters A is physically motivated. Their contributions are described in [8] by:

$$U_{act} = A \cdot ln\left(\frac{i}{i_0}\right) = \frac{R \cdot T_{st}}{2\alpha F} \cdot ln\left(\frac{i}{i_0}\right) \tag{5}$$

where i is the current density, i_0 is the exchange current density representing the reaction rate at the thermodynamic equilibrium, and α is the charge transfer coefficient (system specific).

Amphlett [1] then added the influence of oxygen concentration using the parametric expression:

$$U_{act} = \xi_1 + \xi_2 \cdot T_{st} + \xi_3 \cdot T_{st}(ln(i) + \xi_4 \cdot ln(C_{O_2})) \tag{6}$$

where C_{O_2} is the oxygen concentration at the membrane which is calculated using the channel oxygen partial pressure [1]:

$$C_{O_2} = p_{O_2} \cdot 1.97 \cdot 10^5 \cdot e^{498/T_{st}}. \tag{7}$$

At open circuit, equation (6) can not be parameterized due to the logarithmic current density term. As a result (6) is modified:

$$U_{act} = U_{0,act} + U_a \cdot (1 - e^{-C_1 \cdot i}) \tag{8}$$

where U_{0act} is the current independent part and U_a the current dependent part of the activation loss:

$$U_{0act} = \chi_1 + \chi_2 \cdot T_{st} + \chi_3 \cdot ln(p_{O_2})$$
$$U_a = \chi_4 \cdot T_{st}.$$

The parameters $C_1, \chi_1, \chi_2, \chi_3$, and χ_4 are identified with experimental data. Note here that the open circuit voltage, $U(i = 0)$, (as explained in Fig. 4) is:

$$U(i = 0) = E - U_{0act}.$$

The ohmic loss represents the linear part of the polarization curve and is influenced by proton-flow-resistance in the membrane. This membrane resistance is a function of current, temperature, and membrane water content, λ_m, which varies from 0 to 14, where 0 corresponds to relative humidity of 0% and 14 to 100%, respectively [16]. The ohmic loss then becomes

$$U_{ohmic} = \frac{t_m}{(b_{11} \cdot \lambda_m - b_{12}) \cdot exp\left(b_2\left(\frac{1}{303} - \frac{1}{T_{st}}\right)\right)} \cdot i \tag{9}$$

where t_m is the membrane thickness, b_{12}, b_2, are taken form [13], b_{11} needs identification after assuming $\lambda_m = 14$ due to the experimental conditions and our data set.

2 MODEL ASSUMPTIONS AND INPUTS

Cell-to-cell voltage measurements in a multiple-cell stack show spatial variation. This spatial variation results form the distributed nature of the temperature T, the humidity ϕ, the partial pressures p_{H_2} and p_{O_2}, and the oxygen mole fraction y_{O_2} through the stack. These variables will be closer discussed in this section. Additionally measurements of these variables at the membrane surface of each cell are cumbersome. As an alternative, these variables are assumed to be the arithmetic average of the manifold inlet and outlet values. The voltage model is parameterized with the averaged variables:

$$p_{ca} = \frac{p_{ca,in} + p_{ca,out}}{2} \qquad p_{an} = \frac{p_{an,in} + p_{an,out}}{2} \tag{10}$$

$$T_{ca} = \frac{T_{ca,in} + T_{ca,out}}{2} \qquad T_{an} = \frac{T_{an,in} + T_{an,out}}{2} \tag{11}$$

$$\phi_{ca} = \frac{\phi_{ca,in} + 1}{2} \qquad \phi_{an} = \frac{\phi_{an,in} + 1}{2} \tag{12}$$

where ϕ is the relative humidity. A statistical analysis of cell-voltage measurements will justify this lumped parameter approach. The anode and cathode outlet are assumed to be fully humidified ($\phi_{out} = 1$).

The hydrogen partial pressure is defined by:

$$p_{H_2} = p_{an} - \phi_{an} \cdot p_{sat}(T_{an}) \tag{13}$$

where the vapor saturation pressure, p_{sat}, is a function of temperature.

The oxygen partial fraction is determined after taking into account that the air in the cathode contains oxygen, nitrogen, and vapor. The average oxygen partial pressure is calculated with

$$p_{O_2} = y_{O_2} \cdot \Big(p_{ca} - \phi_{ca} \cdot p_{sat}(T_{ca}) \Big) \tag{14}$$

where the average oxygen mole fraction, y_{O_2}, and dry air is calculated using

$$y_{O_2} = \frac{(2 \cdot \lambda - 1)}{2 \cdot \lambda} \cdot y_{O_2,in} \tag{15}$$

with $y_{O_2,in}$=0.21 the mole fraction of oxygen in dry air at the inlet, and the air excess ratio λ which is calculated from:

$$\lambda = \frac{y_{O_2,in} \cdot 4 \cdot F \cdot W_{air,in}}{n_c \cdot M_{mol,air} \cdot I} \tag{16}$$

where $W_{air,in}$ is air flow at the cathode inlet, n_c the number of cells, $M_{mol,air}$ the molar mass of dry air.

3 PARAMETERIZATION

Here we describe the experimental setup and methodology for parameterizing the polarization model.

For the identification the average cell voltage U_{ave} is used. The average cell voltage is then defined by:

$$U_{ave} = \frac{U_{st}}{n_c} \tag{17}$$

where U_{st} is the measured total stack voltage. The polarization is expressed for a single cell.

3.1 Experimental Hardware

Fig. 1 describes the system configuration for all tests mentioned in this paper. The fuel cell stack installed at the Fuel Cell Laboratory at the University of Michigan contains 24 cells in series with a cell active area of 300 cm^2. The continuous power output of the stack is 1.4 kW. The operating temperature range is from 50°C to 65°C. The fuel cell contains 35 μm thick GORE^{TM}

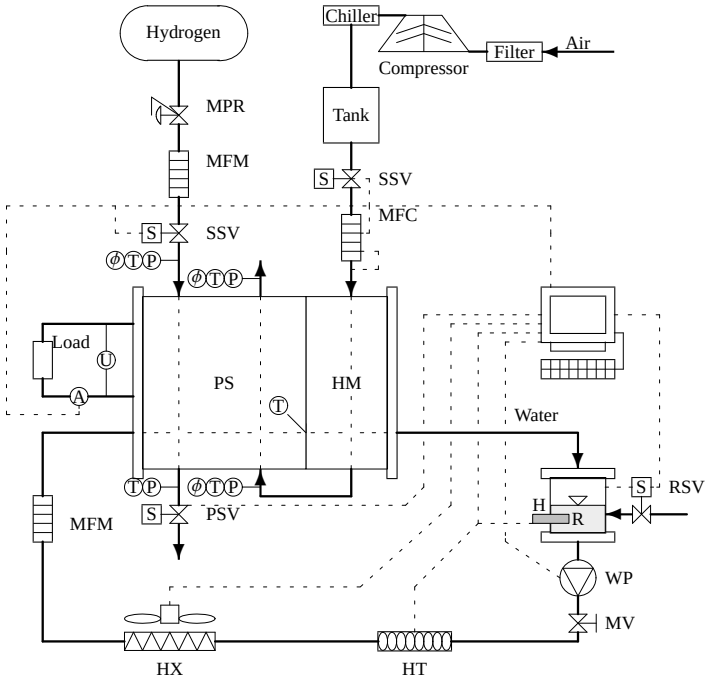

Figure 1: **System configuration, some actuators and sensors:** The dashed lines represent the communication between devices and the computer. **HM** is the humidifier, **PS** the power section, **R** the reservoir, **MPR** the manual pressure regulator, **H** the heater (AC), **HT** the heat tape, **HX** the heat exchanger and fan, **MFC** the mass flow controller, **MV** the manual valve, **PSV** the purge solenoid valve, **SSV** supply solenoid valves, **WP** the water pump, **A** the ampere meter, **MFM** the mass flow meter, **P** pressure sensors, **T** temperature sensors, ϕ humidity sensors, and **U** the stack voltage.

PRIMERA® Series 5620 polymer electrolyte membranes. [1] The diffusion layers are version 3 ETek^{TM} ELATs, and the flow fields are machined into graphite plates.

Compressed pure hydrogen is stored in a cylinder. The anode inlet pressure is regulated with a manual pressure regulator to 3 psig (1.2 bar). The hydrogen path through the anode is dead-ended with a purge solenoid valve that is periodically opened to remove liquid water from the anode. The event of opening anode outlet valve is referred to as “purge”.

The flow of dry oil-less air is controlled with a mass flow controller (MFC) containing an internal PID controller for air flow regulation. The computer sends a mass flow demand to the MFC, based on a desired air excess ratio, λ, and current, I. The dry air outers the humidification section (HM) and then enters

[1] The fuel cell was purchased from the Schatz Energy Research Center at Humboldt State University.

the power section (PS) of the stack.

The cooling loop fulfills two functions: humidification of the air and regulation of the stack temperature. The water temperature regulation is achieved with a heat-exchanger (HX) and on-off fan control for cooling and heating tapes (HT) for heating. The controlled temperature is the coolant water temperature exiting the stack power section (PS).

In Fig. 1 capital letters in a circle are displayed. They represent measurement points. Two resistive temperature devises (RTD) measure the coolant temperatures at the inlet and outlet of the power section with -40 to 85 °C range and ± 0.3 °C accuracy. An MKS type 1559A air mass flow controller (co-located sensor) with range 20-200 slm[2] ± 2 slm accuracy, and 0.5 s time constant is installed upstream of the cathode inlet. A Hastings HFM201 hydrogen mass flow meter (MFM) with 0-100 slm range, ±1 slm, and 2 s settling time is installed upstream of the anode inlet. Three Omega PX4202-005G5V pressure transducers with 0-5 psig range, ±0.012 psig accuracy and 10 ms time constant are used at the cathode inlet/outlet and the anode outlet. An Omega PX603 pressure transducer with 0-30 psig range, ±0.12 psig accuracy and 5 ms time constant is used at the anode inlet. Two relative humidity sensors are installed in the inlet of the anode and the cathode. The current drawn from the stack is controlled and measured with a Dynaload RBL488 electronic load with 0-400 A range (±0.015 A). Individual cell voltages are measured with 0-1200 mV/cell (± 1 mV/cell). Data logging occurs at 2Hz or higher frequency.

3.2 Experimental Methodology

The voltage model is tuned by controlling three inputs, namely the ratio, λ, the current, I, and the stack temperature, T_{st}. I is measured with the ampere meter according to Fig. 1 and T_{st} corresponds to the coolant water temperature at the power section's outlet. Fig. 2 shows the average cell voltage output, U_{ave}, as a function of the three mentioned inputs.

The fuel cell stack is flow-controlled. The air excess ratio is kept at a constant value, not the oxygen partial pressure. Hence, oxygen partial pressure changes at different current levels, I, for constant temperature, T_{st}, and air ratio, λ. The anode inlet total pressure remains constant throughout the experiment so we have to rely on the theoretical dependency of cell voltage to hydrogen pressure. Coolant temperature changes in a bounded range around the temperature set point due to heater, H, heat tape, HT, and heat exchanger, HX, activities.

The set of quasi-static-current measurements comprised of the following conditions. The range of air excess ratio tested was $\lambda \in [2, 2.5, 3]$, for the temperature $T_{st} \in [50, 60, 65]$ °C, and for the current $I \in [0, 15, 30, 45, 60, 75, 90]$ A.

[2]Standard liters per minute (slm) are the units used by the manufacturer. Although SI units are used in the rest of this article, the instrument specifications are quoted with the manufacturer's units.

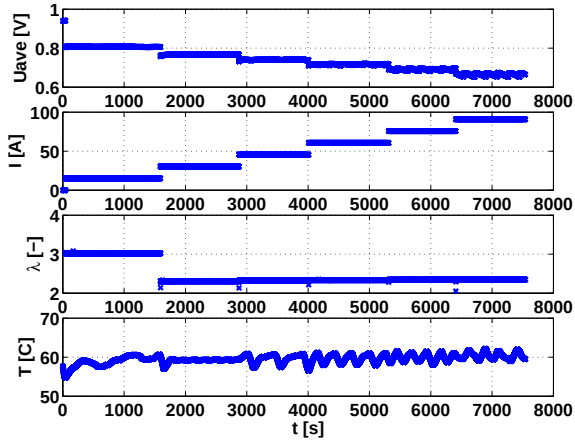

Figure 2: This figure shows some collected data. The first line shows the average cell voltage as a function of experimental time with the corresponding controlled inputs I, λ, and T_{st}. The ranges of λ, and T_{st} are not large.

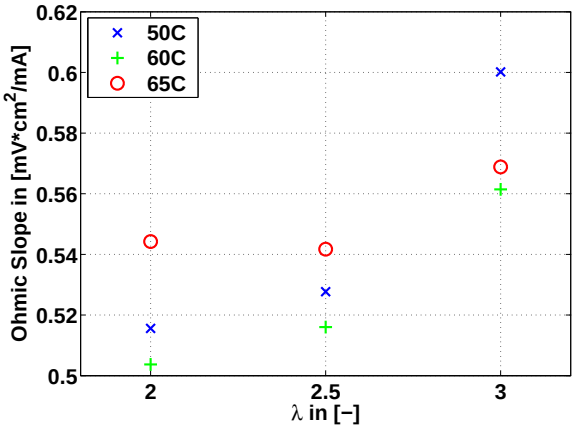

Figure 3: Ohmic slope as a function of temperature and air excess ratio.

3.3 Ohmic loss

The ohmic overvoltage is a function of temperature and current density (9). By comparing the stack voltage measurements as a function of current density for a given temperature and air excess ratio we found that voltage is a linear function of current density at $i \geq 100$ mA/cm^2, indicating the beginning of the ohmic region.

Linear least square regression was applied to find nine different slopes for temperature set points [50, 60, 65] °C, and air excess ratios [2, 2.5, 3] covering each current range from 100 mA/cm^2 to 200 mA/cm^2. Outliers in the data were removed. Fig. 3 plots the calculated slope of the polarization curve at a given temperature and air excess ratio. In this form the slope

represents the cell voltage drop per unit current density.

Amphletts's voltage equation [1] suggests that the ohmic slope decreases with increasing temperature. In Fig. 3 one clearly sees, the ohmic slope tends to increase as air excess ratio increases. However, there is not a consistent monotonic relationship for the range of temperature and air excess ratios tested. The slope variation due to temperature changes is small. Springer's [16] basis function for ohmic loss does not indicate any influence of p_{O_2} (or λ) on the slope. However, there is an oxygen partial pressure p_{O_2} related influence on polarization in the activation overvoltage. Higher pressure decreases U_a, which indirectly influences the slope.

The ohmic slope becomes the average of all nine sets (A set is the data with a constant air ration λ and temperature T_{st}).

The average ohmic slope, B_1, was found to be:

$$B_1 = 5.4215 \cdot 10^{-4}. \tag{18}$$

Where B_1 is in V·cm^2/mA. Relating the ohmic slope to Eqn. (9),

$$B_1 = \frac{t_m}{(b_{11} \cdot \lambda_m - b_{12}) \cdot exp\left(b_2\left(\frac{1}{303} - \frac{1}{T_{st}}\right)\right)}. \tag{19}$$

The median temperature for the data sets was $T_{st} = 331.48$ K. Assuming the membranes are fully humidified (λ_m=14), the membrane thickness $t_m = 3.5 \cdot 10^{-5}$ m, and using $b_{12} = 3.26$ mA/(V·cm) and $b_2 = 350$ from [16], Eqn. (19) can be rearranged to find the parameter $b_{11} = 0.65041$ V·cm^2/ mA.

Note, the influence of membrane water content λ_m could not be directly parameterized because experiments under sub-saturated conditions were not performed. However the polarization must include the membrane water content to show the influence of membrane dehydration on the voltage equation.

3.4 Activation Loss

Parameterization of the polarization model for the activation loss, U_{act}, in the current density range $i \in [0, 100]$ mA/cm^2 is shown in this section. The activation region contains an initial drop at zero current combined with an exponential decreasing function of current (Fig. 4). To force the activation loss to be constant at current densities greater than 100 mA/cm^2 the current rate constant C_1 in Eqn. (8) was tuned to be $C_1 = 0.05$ cm^2/mA.

First, E, is calculated using Eqn. (2). Then, the parameters of the activation loss are tuned. $U_{0,act}$ is the difference between the theoretical open circuit voltage, E, and the median of the average-voltage measurements at zero current. The relationship between $U_{0,act}$ and E is as shown in Fig. 4. The small p_{O_2}-range in data limits the ability to identify χ_3. Nevertheless it is crucial to incorporate the influence of p_{O_2} in the activation to adequately

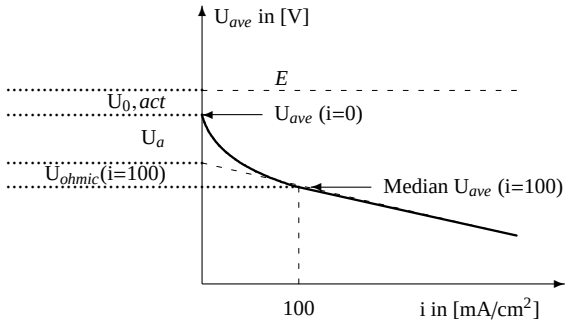

Figure 4: Relationship of activation parameters

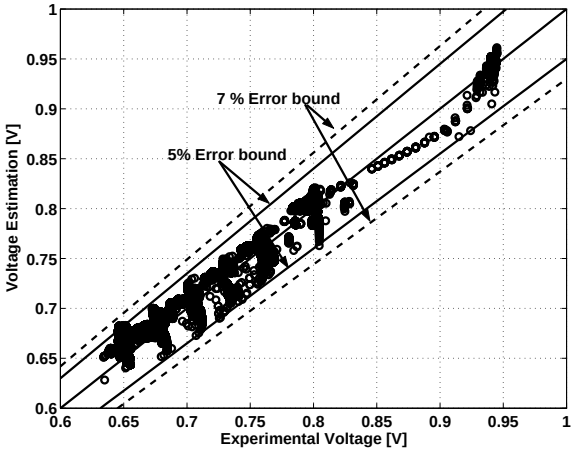

Figure 5: Parity plot of experimental versus estimated voltage.

capture the dynamics associated with oxygen starvation. A linear least squares regression was used to determine the parameters χ_1, χ_2 and χ_3 of Eqn. (8) to describe the relationship of $U_{0,act}$ on T_{st} and p_{O_2}. The following relationship was identified:

$$U_{0act} = 0.7466 - 2.338 \cdot 10^{-5} \cdot T_{st} - 4.739 \cdot 10^{-2} \cdot ln(p_{O_2}). \tag{20}$$

The parameter χ_4 is fitted based on Eqn. (20) for U_{0act}, the measured cell voltage median at 100 mA/cm^2, $U_{ave}(i = 100)$, and the predicted ohmic overvoltage at 100 mA/cm^2, $U_{ohmic}(i = 100)$, calculated from Eqn. (18), using the relation:

$$\begin{aligned} \chi_4 \cdot T_{st} = & E(p_{H_2}, p_{O_2}, T_{st}) - U_{0act}(p_{O_2}, T_{st}) \\ & - U_{ohmic}(i = 100) - U_{ave}(i = 100). \end{aligned} \tag{21}$$

The following relationship was identified:

$$U_a = 3.416 \cdot 10^{-4} \cdot T_{st}. \tag{22}$$

A sensitivity analysis of the parameters χ_1 through χ_4 showed that variations of the coefficient associated with the oxygen partial pressure, χ_3, impact the voltage considerably.

3.5 Identified Polarization

The overall voltage model equation in V as a function of current density i in mA/cm^2, p_{O_2} in Pa, p_{H_2} in Pa, t_m in m, and T_{st} in K was experimentally calibrated, resulting in

$$\begin{aligned} U_{ave} =& 1.23 - 2.30 \cdot 10^{-4} \cdot (T_{st} - 298.15) \\ & + 4.3 \cdot 10^{-5} \cdot T_{st} \cdot ln\left(\frac{p_{H_2} \cdot p_{O_2}^{0.5}}{(101325)^{1.5}}\right) \\ & -0.7466 + 2.338 \cdot 10^{-5} \cdot T_{st} + 4.739 \cdot 10^{-2} \cdot ln(p_{O_2}) \\ & -3.416 \cdot 10^{-4} \cdot T_{st} \cdot (1 - e^{-0.05 \cdot i}) \\ & - \frac{0.906 \cdot t_m}{(0.65041 \cdot \lambda_m - 3.26)} \cdot i. \end{aligned} \quad (23)$$

In Fig. 5 a parity plot compares the voltage-estimation to the average-voltage measurements. A maximum error of 7% occurred for four data sets at 75 and 90A (data not used for identification). The error at high current density (low voltage) is more significant than at low current density (high voltage), perhaps due the degree of electrode flooding.

4 SENSITIVITY AND STATISTICAL ANALYSIS

We present a graphical sensitivity analysis of the influence of inputs on the estimated polarization as a function of current density. We then provide a statistical analysis on the measured cell voltages. Finally we provide an analytical assessment of the impact of sensor resolution on the estimated polarization.

4.1 Influence of Inputs

The input variables (T_{st}, λ_m, p_{O_2}, p_{H_2}) were varied to examine their influence on the estimated polarization, some are shown in Fig. 6, 7, and 8. The stack temperature had the smallest influence on the estimated voltage, with the membrane water content having the greatest influence. When the cell dehydrates (λ_m = 8 corresponds to a membrane relative humidity of 83%), the membrane resistance increases causing a decrease in cell voltage. Although this trend is physically justified and has been observed in experiment, we cannot validate the exact mathematical relation because we cannot measure the exact membrane water content λ_m. As expected, the influence of the reactant pressures or cell temperature impacts the OCV and activation loss, only, resulting in a constant slope at current density above 100 mA/cm^2. The membrane water content, however impacts the ohmic loss and thus influences the slope in the ohmic region.

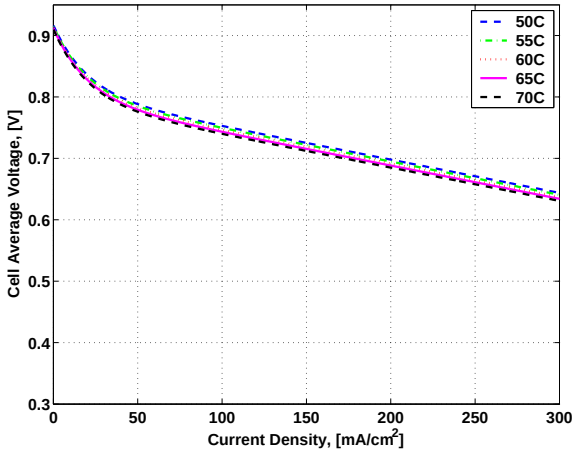

Figure 6: Influence of T_{st}

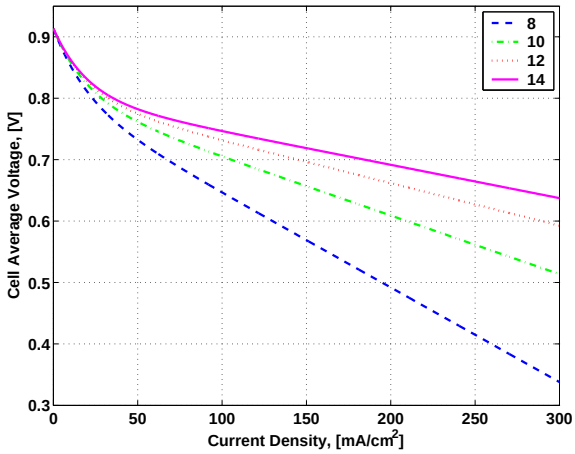

Figure 7: Influence of λ_m

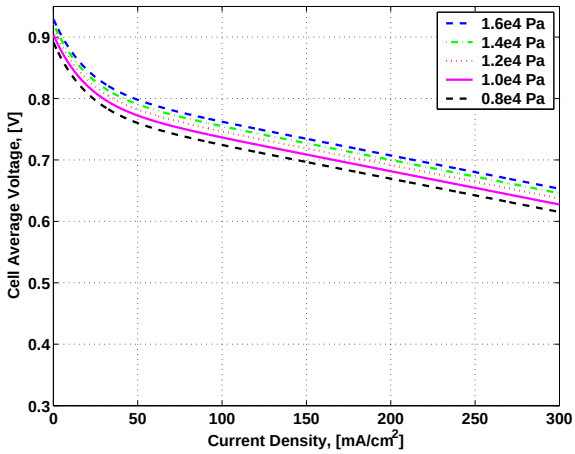

Figure 8: Influence of p_{O_2}

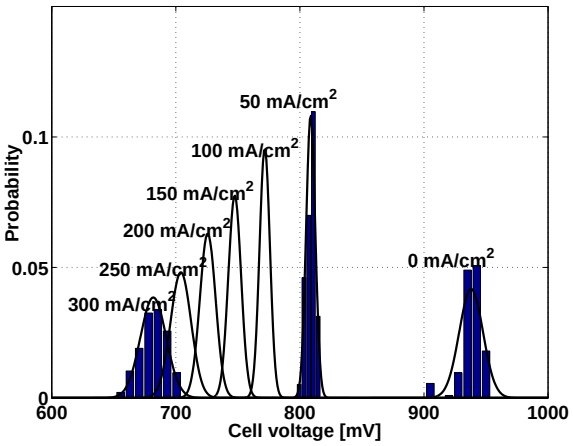

Figure 9: Bell curves for $i \in [0, 50, 100, 150, 200, 250, 300]$ mA/cm^2

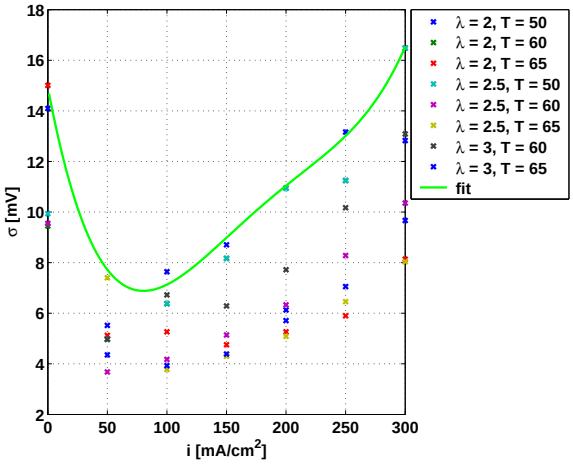

Figure 10: Cell-voltage standard error σ(i) in mV, i in mA/cm^2

The influence of the oxygen partial pressure on cell voltage (through the OCV and activation loss) is important when considering reactant dynamics. For low oxygen partial pressure, the logarithmic term in the Nernst equation becomes negative. Although this is the right trend, experiments with such severe starvation were not performed.

Anode pressure was kept constant during experiments. Thus, influence of hydrogen partial pressure was not measured. However, p_{H_2} affects the open circuit voltage through the Nernst equation and shows a similar effect as p_{O_2}.

4.2 Statistical Analysis

Cell-voltages vary due to pressure, temperature, and humidity changes along the stack's flow channels. Fig. 9 shows the distribution plots for cell-voltage measurements at different current densities and at λ= 2.5, T_{st}= 60°C. The actual bar plots of the cell-voltage-measurements are shown with the bell curves for $i \in [0, 50, 300]$ mA/cm^2 to verify the normal distribution.

The standard deviation associated with the cell-to-cell voltage variation, shown in Fig. 10, is large at 0 current, decreases for 50 mA/cm^2 and increases again as a function of current density. A difference smaller than 2.7% should be expected from cell-to-cell based on the observed standard deviation and the average voltage value. This error is small enough to justify polarization parametrization based on average voltage calculation.

There is no pattern in the standard deviation observable as a function of λ or T_{st} similar to the one identified by Rodatz [14]. A fifth order polynomial fits the maximum standard deviation as a function of current density.

$$\begin{aligned}\sigma(i) = {} & 1.2938 \cdot 10^{-8} \cdot i^4 - 9.4521 \cdot 10^{-6} \cdot i^3 \\ & + 2.5156 \cdot 10^{-3} \cdot i^2 - 0.2479 \cdot i + 14.934\end{aligned} \tag{24}$$

Eqn. (24) serves as a voltage uncertainty model, where i is in [mA/cm^2], and σ in [mV] and is shown with the solid line in Fig. 10.

4.3 Sensor Resolution

When utilizing measured variables for parameter identification the sensor resolution should be considered. The polarization model is a function of measured variables (T_{st}, i) or variables calculated using measurements (p_{O_2}, p_{H_2}) therefore the analytical error propagation is investigated using

$$\begin{aligned}\Delta U_{ave} = {} & \left|\frac{\partial U_{st}}{\partial T_{st}} \cdot \Delta T_{st}\right| + \left|\frac{\partial U_{st}}{\partial p_{H_2}} \cdot \Delta p_{H_2}\right| \\ & + \left|\frac{\partial U_{ave}}{\partial p_{O_2}} \cdot \Delta p_{O_2}\right| + \left|\frac{\partial U_{st}}{\partial i} \cdot \Delta i\right| \\ = {} & 1.81 \cdot 10^{-4} + 0 + 0 + 3.12 \cdot 10^{-4} \\ = {} & 4.93 \cdot 10^{-4}\end{aligned} \tag{25}$$

where ΔU_{ave} is in V. As operating point used here is T_{st} = 333 K, p_{H_2} = 80000 Pa, p_{O_2} = 12000 Pa, and i = 300 mA/cm^2. The calculation showed that the maximum error associated with the sensor resolution occurs at 300 mA/cm^2. The errors due to pressure resolution is so small that it can be neglected. The sensor resolution are taken from section 3.1. To derive a relative value, the maximum measurement error is divided by the minimum cell voltage (650 mV) at open circuit. The maximum measurement error is then 0.7%, which is small compared to the error (7%) introduced by the fitting of the average polarization as shown in Fig. 5.

5 DYNAMIC VOLTAGE RESPONSE

Although we have demonstrated the ability of the derived static polarization model to capture our quasi-static experimental results, the model developed here must be combined with a additional dynamic equations that describe the cell reactant and water dynamics. The model augmentation is necessary to predict voltage transients associated with reactant depletion that occurs during fast changes in current drawn from the fuel cell and electrode flooding that occurs during liquid water accumulation. The model by McKay et al. [10] is a two-phase one-dimensional model describing reactant and water dynamics by discretizing the gas diffusion layer (GDL). The model in [10] calculates species concentrations across the GDL and the degree of flooding in the electrodes. The p_{O_2} and p_{H_2} at the catalyst surface (instead of the channel) are now inputs to our polarization model. Moreover, we feed the apparent density i_{app} (instead of the commanded i given in (4)) to the polarization model.

Using the catalyst reactant concentrations and the apparent current density has implications in the predicting ability of the derived static model. In particular we show with two experiments in Fig. 11 and 12 (subplot 1) that the reactant concentrations are lower at the catalyst surfaces than in the flow fields, especially when liquid water saturation impedes the oxygen transport as in Fig 11. Additionally, the oxygen concentration transients are now slower and of a different magnitude at the catalyst interface than in the channels due to the time lag associated with transport through the GDL. As a result we predict better the transients associated with oxygen starvation but we under-predict the overall steady-state voltage. Using the apparent current density has a more profound effect to the voltage prediction that is explained in detail next.

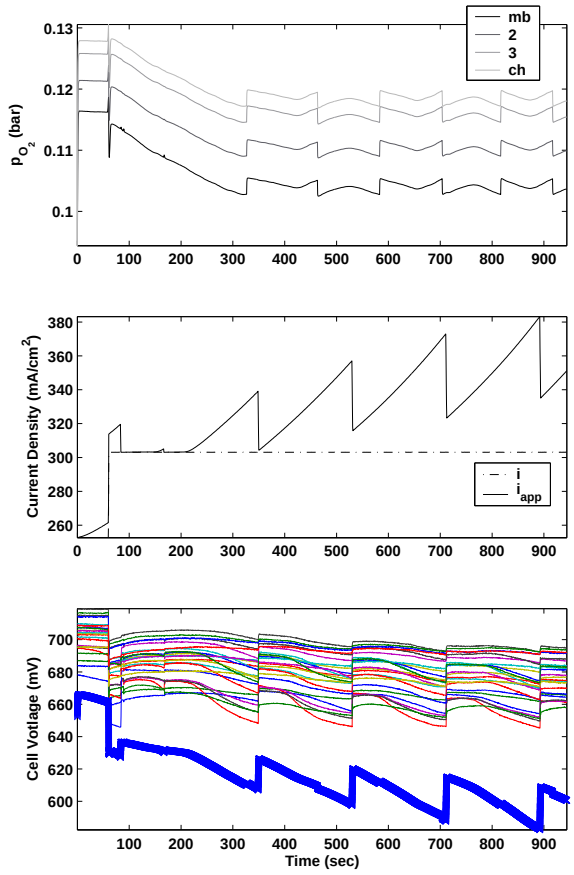

Figure 11: Cell-voltage-responses when anode is flooding, thin lines correspond to measurements, the thick line is the model prediction.

5.1 Reactant Depletion

The polarization model was parameterized using channel properties. The variables influencing the actual cell voltage, however are located at the membrane-catalyst interface. Following a step increase in current, shown in Fig. 11, oxygen depletion at the catalyst layer is more significant than in the cathode channel. As a result, the oxygen partial pressure decreases rapidly causing a distinct drop in the cell voltage until the oxygen is replenished and the air excess ratio returns to the setpoint. Thus, the static voltage-equation with dynamic inputs captures the voltage response during oxygen depletion.

5.2 Electrode Flooding

Flooding appears, when the production or transport of vapor overcomes the ability of the water vapor to diffuse through the GDL. The vapor then supersaturates and condenses. The liquid water then partially coats the catalyst layer, reducing the cell active area. As a result, the apparent current density, i_{app}, increases due to the decreased active area. Using the apparent current density as an input to the polarization model, the impact of flooding on cell voltage can be examined.

Fig. 11 shows the measured cell voltage (thin lines) and the model prediction (thick lines) at i= 300 mA/cm^2. The middle subplot indicates the apparent current density, i_{app}, compared to the nominal current density. As explained in section 3.1, the anode is periodically purged to remove liquid water. These purging events are noted by the sharp increase in voltage following a slower overall voltage decay. Different degrees of flooding (changing cell active area) lead to the saw-tooth pattern of the apparent current density. Of most importance, the static voltage equation captures the dynamic response associated with electrode flooding.

Fig. 12 shows the measured and predicted cell voltages at lower current density, when the degree of flooding is less significant. Notice the apparent current density is equal to the nominal current density following a purge event, indicating that reactants are no longer being obstructed from the catalyst layer. The trend in voltage between purging events is captured well.

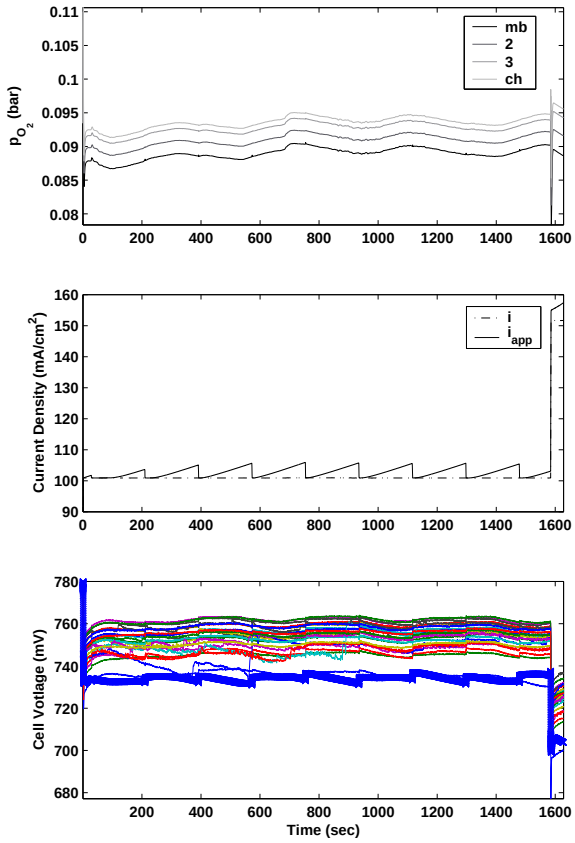

Figure 12: Cell voltage response under better managed electrode flooding conditions.

6 CONCLUSION

We present a detailed model of cell polarization that depends on reactant partial pressure, temperature, membrane water content and current density. The model was calibrated and experimentally validated for a low pressure 24 cell, 300 cm^2 PEM fuel cell stack. The maximum error in the voltage was 7%. A model was developed to describe the standard deviation of 2.7%. Rather than incorporating dynamics in the voltage equation, we demonstrate the ability of this static polarization equation to capture reactant and flooding dynamics when coupled with a dynamic lumped parameter model of the gas channels, diffusion layer and membrane.

REFERENCES

[1] J. Amphlett, R. Baumert, R. Mann, B. Pepply, P. Roberge, and A. Rodrigues. Parametric modelling of the performance of a 5-kW proton-exchange fuel cell stack. *Journal of Power Sources*, (49):349–356, 1994.

[2] S. Busquet, C. Hubert, J. Labbé, D. Mayer, and R. Metkemeijer. A new approach to empirical electrical modelling for a fuel cell, an electrolyzer or a regenerative fuel cell. *Journal of Power Sources*, (134):41–48, 2004.

[3] M. Ciureanu and R. Roberge. Electrochemical impedance study of PEM fuel cells. Experimental diagnostics and modelling of air cathodes. *Journal of Physical Chemistry*, (105):3531–3539, 2001.

[4] J. Correa, F. Farre, L. Canha, and M. Simoes. An electrochemical-based fuel-cell model suitable for electrical engineering automation approach. *IEEE Transactions*, 51(5):1103– 1112, Oct. 2004.

[5] J. Kim, S. Lee, and S. Srinivasan. Modelling of proton exchange membrane fuel cell performance with an empirical equation. *Journal of Power Sources*, (135):110–121, 2004.

[6] S. Kim, S. Shimpalee, and J. VanZee. The effect of stoichiometry on dynamic behavior of a proton exchange membrane fuel cell (PEMFC) during load change. *Journal of Electrochemical Society*, 142(8):2670–2674, 1995.

[7] P. Kwangjin and B. Joongmyen. Study of dynamic behavior for PEMFC stack. In *Proceedings of FUELCELL 2005*, volume FUELCELL2005-74067, Department of mechanical Engineering Korea Advanced Institute of Science and Technology (KAIST), Daejeon, South Korea, May 2005. Third International Conference on Fuel Cell Science, Engineering and Technology, ASME.

[8] J. Larminie and D. Dick. *Fuel Cell Systems Explained*. Wiley, West Sussex, England, 2nd edition, 2003.

[9] R. Mann, J. Amphlett, M. Hopper, H. Jensen, B. Peppley, and P. Roberge. Development and application of a generalized steady-state electrochemical model for a PEM fuel cell. *Journal of Power Sources*, (86):173–180, 2000.

[10] D. McKay, W. Ott, and A. Stefanopoulou. Modelling, parameter identification, and validation of water dynamics for a fuel cell stack. In *Proceedings of IMECE'05*, volume IMCE2005-81484, Fuel Cell Control Laboratory, Epautement of Mechanical Engineering, University of Michigan, Ann Arbor MI 28109, November 2005. 2005 ASME International Mechanical Engineering Congress and Exposition, ASME.

[11] D. McKay and A. Stefanopoulou. Parametrization and validation of a lumped parameter diffusion model for fuel cell stack membrane humidity estimation. *Proceedings of 2004 American Control Conference, Boston, MA*, 814-821, 2003.

[12] P. Pathapati, X. Xue, and J. Tan. A new dynamic model for predicting transient phenomena in a PEM fuel cell system. *Renewable Energy*, (30):1–22, 2004.

[13] J. Pukrushpan, A. Stefanopoulou, and H. Peng. *Control of Fuel Cell Systems: Principles, Modelling, Analysis, and Feedback Design*. Springer, London, 2004.

[14] P. Rodatz. *Dynamics of the Polymer Electrolyte Fuel Cell*, volume Diss. ETH Nr.15320. Measurement and Control Laboratory, Swiss Federal Institute of Technology, Zurich, ETH Zentrum, Zurich, Switzerland, 2003.

[15] P. Rodatz, C. Onder, and L. Guzella. Air supply system of a PEMFC stack dynamic model. *Fuel Cells*, 5(1):126–132, Febuary 2005. Measurement and Control Laboratory, Swiss Federal Institute of Technology, Zurich, ETH Zentrum.

[16] T. Springer, T. Zawodzinski, and S. Goffesfeld. Polymer electrolyte fuel cell model. *Journal of Electrochemical Society*, 138(8):2334–2342, 1991.

[17] L. Wang, A. Husar, T. Zhou, and L. Hangton. A parametric study of PEM fuel cell performances. *International Journal of Hydrogen Energy*, (28):1263–1272, 2003.